Spatial-size scaling of pedestrian groups under growing density conditions

Francesco Zanlungo,* Dražen Brščić, and Takayuki Kanda
IRC-ATR, Kyoto, Japan and JST CREST, Tokyo, Japan

(Received 17 February 2015; revised manuscript received 23 February 2015; published 19 June 2015)

We study the dependence on crowd density of the spatial size, configuration, and velocity of pedestrian social groups. We find that, in the investigated density range, the extension of pedestrian groups in the direction orthogonal to that of motion decreases linearly with the pedestrian density around them, both for two- and three-person groups. Furthermore, we observe that at all densities, three-person groups walk slower than two-person groups, and the latter are slower than individual pedestrians, the differences in velocities being weakly affected by density. Finally, we observe that three-person groups walk in a V-shaped formation regardless of density, with a distance between the pedestrians in the front and back again almost independent of density, although the configuration appears to be less stable at higher densities. These findings may facilitate the development of more realistic crowd dynamics models and simulators.

DOI: 10.1103/PhysRevE.91.062810 PACS number(s): 89.65.Ef, 89.75.−k, 89.20.−a

I. INTRODUCTION

Crowd dynamics modeling is an active and promising field in which physical science methods, such as molecular dynamics, fluid dynamics, or cellular automata, are applied to social systems [1–9]. Social groups, which represent in some environments up to 85% of the walking population [10,11], may be considered as bound systems composed of individual pedestrians, and thus they represent, to some extent, for the pedestrian crowd what molecules are in a fluid. It should indeed be expected that such groups, walking in a characteristic configuration [10–14] and with slower velocity than pedestrians outside groups [11,14–16], have an important influence on the dynamics of the crowd. Nevertheless, until recent times, their presence has been largely ignored in the development of crowd dynamics models.

In the last few years, a few models describing group dynamics have been introduced [11,17–19] (see also [20] for a recent review of the field), but they often rely on a quite simplistic description of groups, both in their *free-walking* (or *low-density*, $\rho \to 0$) behavior and in their reaction to growing density conditions. For example, a seminal work in the field is [11], which introduces a model describing pedestrian groups as abreast when freely walking, and bending to V and U formations in higher density conditions. While this model explains correctly some features of group behavior, its calibration was performed on only two density values; furthermore, the description of free-walking groups as abreast is in contrast with other qualitative and quantitative observations [10,12,13].

In [14] we introduced a non-Newtonian[1] potential for the dynamics of pedestrian groups *in the low-density limit*. Writing the relative position of two socially interacting pedestrians i and j as $\mathbf{r}_{ij} = (r,\theta)$, where $\theta = 0$ gives the direction to the pedestrians' goal, we made the hypothesis that the discomfort of i due to not being located in the optimal position for social interaction with j is given by

$$\begin{aligned} U_{ij}^{\eta}(r,\theta) &= R(r) + \Theta^{\eta}(\theta), \\ R(r) &= C_r\left(\frac{r}{r_0} + \frac{r_0}{r}\right), \\ \Theta^{\eta}(\theta) &= C_\theta\{(1+\eta)\theta^2 + (1-\eta)[\theta - \mathrm{sgn}(\theta)\pi]^2\}, \end{aligned} \tag{1}$$

where r_0 is the most comfortable interaction distance, and $-1 \leqslant \eta < 0$.[2] Assuming that the acceleration of the pedestrian i due to group dynamics, i.e., to the action of the pedestrian aimed to minimize social interaction discomfort with respect to j, is given by

$$\mathbf{f}_{ij} = -\nabla_i U_{ij}^{\eta}, \tag{2}$$

the model predicts the following:

(i) Two-person groups are slower than individual pedestrians, i.e., naming $v^{(n_g)}$ the average velocity of a group of size n_g, we have

$$v^{(1)} > v^{(2)}. \tag{3}$$

(ii) Three-person groups are even slower, i.e.,

$$v^{(2)} > v^{(3)}, \tag{4}$$

with the following relation holding between the different group velocities:

$$v^{(1)} - v^{(2)} \approx 3(v^{(2)} - v^{(3)}). \tag{5}$$

(iii) Three-person groups walk in a V formation, with the central pedestrian walking slightly behind.

After providing an estimate for what can be considered low-density conditions,[3] we successfully compared our model to Japanese pedestrian real-world data. Furthermore, the predictions regarding group velocity are in good agreement also with the results of [15,16], and thus they appear to have

*zanlungo@atr.jp

[1]Here by non-Newtonian we mean not obeying the third law of dynamics, i.e., $\mathbf{f}_{ij} \neq \mathbf{f}_{ji}$. Refer also to [21] for the importance of such potentials to pedestrian studies.

[2]In Eq. (1), we are assuming that θ takes values in $(-\pi,\pi]$, and using $\mathrm{sgn}(0) = -1$ in order to have a continuous potential. Refer to the original work for details.

[3]Basically, the expected distance to a pedestrian outside the group, or to a wall, has to be considerably larger than the spatial extension of the group.

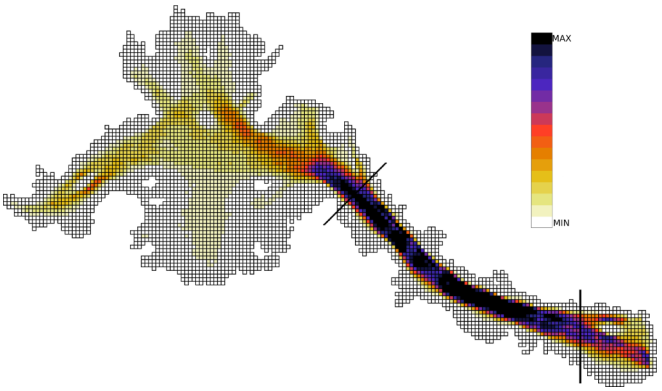

FIG. 1. (Color online) Pedestrian density map of the tracking area. The "corridor," whose data were used for this work, is limited by the black lines. The map uses $A = 0.25$ m^2 sized cells, and averages over positions of pedestrians with velocity $v > 0.5$ m/s, in order to compute density. The figure shows a time average over all data collected on a particular day, namely May 5th 2013.

a cross-cultural value. The model may describe also larger pedestrian groups, predicting that they walk in U formations with central pedestrians slightly behind, in agreement with the observations of [10,11]. Nevertheless, these works used short observation times, thus the stability of these structures could not be assessed. As reported in [13,22], large group structures are unstable, and usually break in stable subgroups of two or three units. We thus believe that larger groups should be modeled through the interactions of their stable subgroup components, and that to attain this end a full understanding of two- and three-person groups has to be reached first.

In the present work, we try to understand, from an empirical point of view, i.e., analyzing a large set of real-world pedestrian data, how the velocity, spatial structure, and extension of two- and three-person groups change beyond the low-density limit.

II. DATA COLLECTION

A. Tracking

The pedestrian trajectories were collected in the Asia and Pacific Trade Center (ATC), a multipurpose building located in the Osaka (Japan) port area. Using three-dimensional (3D) range sensors and the algorithm described in [23], we tracked the position and velocity of pedestrians in a $\approx$900 m^2 area of the building for more than 800 h during a one-year time span, and we video recorded the tracking area using 16 different cameras. The environment, described in detail in [24] and shown in Fig. 1, consists mainly of a large atrium and a long "corridor," and it has a mixed population composed of commuters and local workers (prevalent on working days) and shoppers (prevalent on nonworking days). For the purpose of this work, in order to avoid taking into consideration the effect of architectural features of the environment, such as its width, we use data only from the corridor area (as defined in Fig. 1).[4]

While our tracking system provides us with pedestrian position and velocities at time intervals δt in the order of tens of milliseconds, we average pedestrian positions over time intervals $\Delta t = 0.5$ s to reduce the effect of measurement noise and the influence of pedestrian gait. We obtain pedestrian positions at discrete times k as

$$\mathbf{x}(k\Delta t) = (x(k\Delta t), y(k\Delta t)), \tag{6}$$

and we define pedestrian velocities as

$$\mathbf{v}(k\Delta t) = \{\mathbf{x}(k\Delta t) - \mathbf{x}[(k-1)\Delta t]\}/\Delta t. \tag{7}$$

B. Criteria for data collection

We are interested in groups of pedestrians that are *walking and socially interacting*. To identify them, and to verify their social interaction, we asked one of the coders that we used for our previous work [14] to analyze 24 h of video recording[5] from four different cameras located in the corridor area.[6]

As for the data used in [14], the coder was asked to identify all pedestrian groups, based on any kind of motion or visual cue, and between all groups to identify those pedestrians that were socially interacting. The definition of social interaction was based on conversation and gaze clues [25,26]. Overall she identified 9973 pedestrian groups of sizes from 2 to 21, for a total of 24 565 pedestrians, of which 21 463 (87%) were properly tracked by our system. Pedestrians that were identified as socially interacting did not necessarily interact during the whole tracking time, while pedestrians tracked as not interacting could have been interacting when tracked but not visible from the camera.[7] All the tracking data and annotations used for this work are available at www.irc.atr.jp/sets/groups/.

As we did in [14], we analyzed only *fully interacting groups*, i.e., groups in which at least one of the members was coded as having social interaction with all the other members. We also excluded groups in which wheelchairs or strollers were present.

Regarding the groups that satisfied the above requirements, we used only data points in which all pedestrians in the group have a velocity with magnitude $v_i > 0.5$ m/s,[8] and in which also the overall group velocity satisfies $V = |\sum_{i=1}^{n_g} \mathbf{v}_i|/n_g >$

[4]This corridor, having a width of $\approx$3 m, is considerably narrow compared to the environment studied in [14].

[5]Twelve hours from three different working days, and 12 h from three nonworking days. The specific hours were chosen in such a way to represent the different behavior and density patterns of the environment.

[6]The coder analyzed thus 96 h of video recording and compared them to the tracking data. This is already a very large workload, and for this reason it was impossible either to analyze all the cameras located in the corridor area or to use both coders that worked on the data used in [14].

[7]The coding process was designed to avoid the presence of false positives, while allowing for false negatives. Nevertheless, asking the coder to annotate the exact time of interaction would have increased her workload too greatly. In any case, we removed from our analysis some groups for which the coder explicitly wrote in her annotations that the interaction was extremely short.

[8]As explained in [27], the threshold is chosen in such a way to clearly separate the velocity distribution of walking and standing pedestrians (the latter having in our system a nonzero velocity due to noise and nonwalking body movement), and results are not sensitive to slight modifications to it.

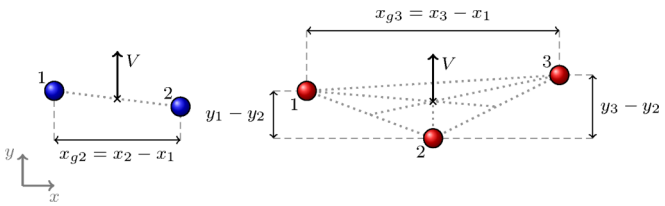

FIG. 2. (Color online) Definition of the two- and three-person group observables.

0.5 m/s.[9] Finally, only data points in which all pedestrians fall inside a square with side 2.5 m centered on the group center were used.[10]

After this filtering process, the data set used for this work consisted of 162 547 observation points of 3305 two-person socially interacting groups, and 21 231 observation points of 602 three-person interacting groups. In what follows, we will refer to this interacting two- and three-person group data set as the "ATC data set."

III. OBSERVABLES

Based on the insight on group behavior obtained in [11,14], in order to analyze the structure and velocity of groups, we may define the following observables (see also Fig. 2).

A. Group center and velocity

Let us consider a group with n_g pedestrians whose positions and velocities are given by vectors $\mathbf{x}_i$, $\mathbf{v}_i$, $1 \leqslant i \leqslant n_g$. Let us define the group center $\mathbf{X}$ and velocity $\mathbf{V}$ as

$$\mathbf{X} \equiv \frac{\sum_{i=1}^{n_g} \mathbf{x}_i}{n_g}, \tag{8}$$

$$\mathbf{V} \equiv \frac{\sum_{i=1}^{n_g} \mathbf{v}_i}{n_g}. \tag{9}$$

It is also useful to define the group walking direction unit vector as

$$\hat{\mathbf{V}} \equiv \frac{\mathbf{V}}{|\mathbf{V}|}. \tag{10}$$

B. Group reference frame

Considering the position of pedestrians with respect to the center, $\mathbf{r}_i \equiv \mathbf{x}_i - \mathbf{X}$, we may define their components along and orthogonal to the group velocity as

$$y_i \equiv \mathbf{r}_i \cdot \hat{\mathbf{V}}, \tag{11}$$

$$x_i \equiv (\mathbf{r}_i \wedge \hat{\mathbf{V}}) \cdot \hat{\mathbf{n}}, \tag{12}$$

where $\hat{\mathbf{n}}$ is an outgoing unit vector normal to the walking plane. Finally, we may relabel the pedestrians in such a way to have $x_i \leqslant x_j$ for $i < j$, i.e., x_1 will be the leftmost and x_{n_g} the rightmost pedestrian with respect to the axis determined by the group velocity.

C. Two-person groups

1. Abreast extension

The abreast extension, i.e., orthogonal to the walking direction, of the group may be defined as

$$x_{g2} \equiv x_2 - x_1. \tag{13}$$

2. Walking direction extension

The extension in the direction of walking may be defined as

$$y_{g2} \equiv y_2 - y_1. \tag{14}$$

D. Three-person groups

1. Abreast extension

The abreast extension, i.e., orthogonal to the walking direction, of the group may be defined as

$$x_{g3} \equiv x_3 - x_1. \tag{15}$$

2. Walking direction extension

We define the extension of the group in the walking direction as

$$y_{g3} \equiv (y_3 + y_1 - 2y_2)/2. \tag{16}$$

The advantage of this definition is that it automatically specifies the group configuration, assuming a value $y_{g3} > 0$ for a V formation and a value $y_{g3} < 0$ for a Λ formation with the central pedestrian walking ahead [14].

IV. RESULTS AND DISCUSSION

For all the above observables, we compute the dependence on local density of the average value and of the probability distribution function according to the procedure described in Appendixes A, B, and C.

A. Velocity

Figure 3 shows the density dependence of group velocity $V = |\mathbf{V}|$, for two- ($V = v^{(2)}$) and three- ($V = v^{(3)}$) person groups, compared to the velocity of individuals walking alone ($v^{(1)}$). Surprisingly, $v^{(1)}$ and $v^{(2)}$ assume a maximum around $\rho \approx 0.03$. This may be due to the following: (i) "rush hours," during which pedestrians walk faster even if the density is higher, as reported in [24], and (ii) low-density areas (visible in white in the corridor area of Fig. 1), in which pedestrians may exhibit wandering behavior.

[9]This requirement, introduced to further assure that the pedestrians are moving as a group, was not present in [14], but it changes the results in a negligible way.

[10]This threshold is located in such a way to include the bulk of spatial distributions of interacting pedestrians, and results depend weakly on its specific value. The reason for the introduction of such a threshold was to exclude data points in which the groups had suspended their interaction and spatially separated.

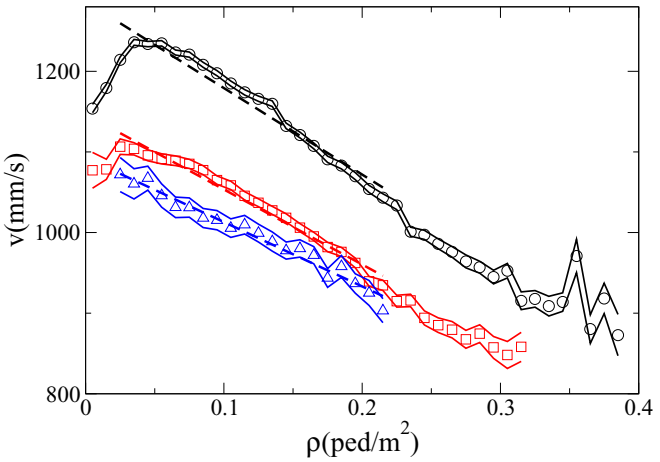

FIG. 3. (Color online) ρ dependence of pedestrian velocity. Individual pedestrians in black circles, two-person groups in red squares, three-person groups in blue triangles. Continuous lines provide standard error confidence intervals, while dashed lines provide a linear fit of the data (limited to the common definition range), given by a law $v^{(i)} = \alpha_i + \beta_i \rho$, with $\alpha_1 = 1.286$ m/s, $\beta_1 = -1.072$ m^3/(ped s), determination coefficient $R_1^2 = 0.949$; $\alpha_2 = 1.147$ m/s, $\beta_2 = -0.931$ m^3/(ped s), $R_2^2 = 0.976$; $\alpha_3 = 1.092$ m/s, $\beta_3 = -0.799$ m^3/(ped s), $R_3^2 = 0.971$.

For $\rho > 0.05$, velocity appears to decrease almost linearly in the observed density range, in a way similar for all group sizes, although the effect appears to be stronger for smaller groups, i.e., individuals are the most affected by density, while three-person groups are the less affected, as shown by the linear fits in Fig. 3. The $\rho \to 0$ results of Eqs. (3) and (4) are valid for all empirical values of ρ for which a comparison between $v^{(1)}$, $v^{(2)}$, and $v^{(3)}$ was possible. Regarding the extension to higher density of the relation of Eq. (5), we may observe that we have for all values of ρ

$$\frac{v^{(1)} - v^{(2)}}{v^{(2)} - v^{(3)}} > 2, \tag{17}$$

with most values between 2 and 4, and a tendency of this ratio to increase with ρ, as shown in Fig. 4. Furthermore, if we perform a linear fit $v^{(i)} = \alpha_i + \beta_i \rho$, as shown in Fig. 3, we obtain

$$\frac{\alpha_1 - \alpha_2}{\alpha_2 - \alpha_3} \approx 2.6, \tag{18}$$

in substantial agreement with the prediction of Eq. (5).[11]

[11]We should nevertheless stress that in the ATC data set, we did not have an explicit coding of individual pedestrians, which, on the other hand, was available for the data set of [14]. We thus followed the same approach that we introduced in [24] to avoid false detections, and we defined as individual pedestrians all pedestrians not coded as part of groups that remained in the environment for at least 8 s and that had a vectorial average velocity (displacement over time) larger than 0.5 m/s (this latter requirement was applied also to two- and three-person groups, although these have been explicitly coded, to avoid a bias in the results concerning velocity averages.). We verified that the results shown in this section are not significantly affected by modifications in these thresholds.

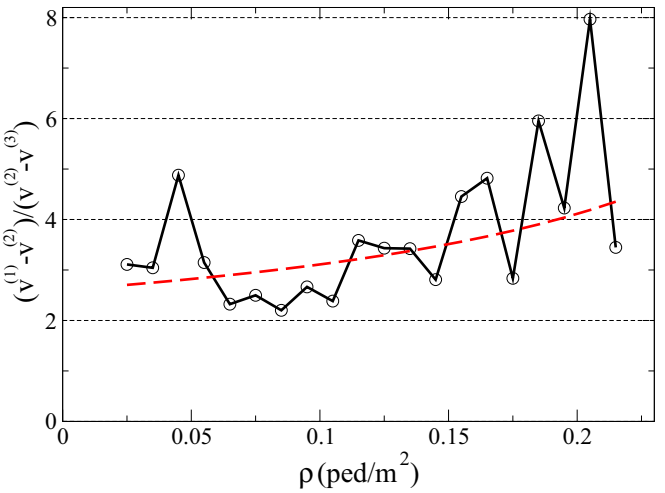

FIG. 4. (Color online) Black and circles: ρ dependence of $(v^{(1)} - v^{(2)})/(v^{(2)} - v^{(3)})$, computed using the average values of Fig. 3. Dashed red: in order to decrease the effect of fluctuations, the same ratio is computed using the linear fits of Fig. 3.

B. Two-person groups

Figure 5 shows the density dependence of the average value of x_{g2} [Eq. (13)], compared to a linear fit of the average value data points.[12] We may see that the abreast extension of the group is reduced with growing density, and that in the studied range the dependence can be reasonably approximated as linear. By examining the probability distributions for x_{g2} in different ρ ranges (Fig. 6), we may notice that this effect is due to a progressive, even if moderate, displacement of the peak position, and to a stronger reduction of the high x tail, to which corresponds an increased probability to have $x \approx 0$ (pedestrians have a higher probability of following each other).

[12]Given by $x_{g2} = \alpha + \beta\rho$, with $\alpha = 0.646$ m and $\beta = -0.538$ m^3/ped, and determination coefficient $R^2 = 0.977$.

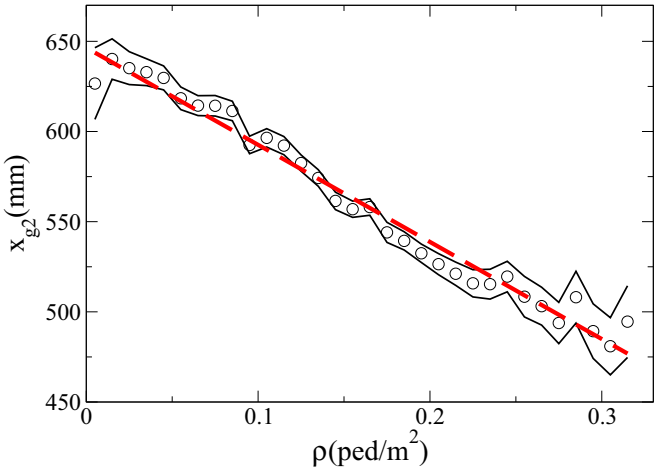

FIG. 5. (Color online) ρ dependence of x_{g2} [Eq. (13)], in black circles, compared to a linear fit of the data (dashed red). Continuous lines provide standard error confidence intervals.

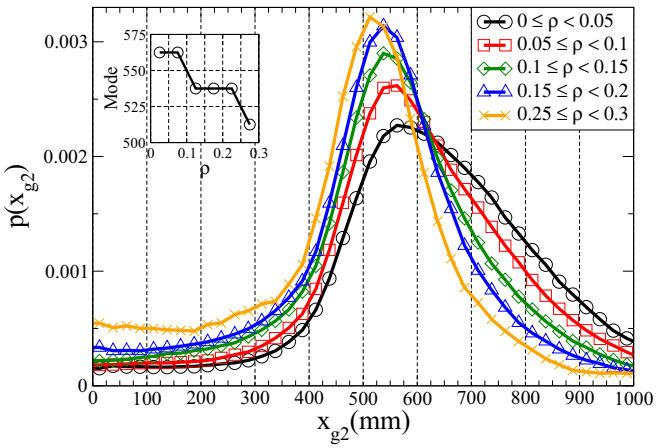

FIG. 6. (Color online) Probability distributions for x_{g2} [Eq. (13)], in different ρ ranges. The inset graph shows the position of the mode as a function of ρ. A one-way ANOVA analysis shows that the distributions in the figure are different in a statistically significant way ($p < 10^{-8}$).

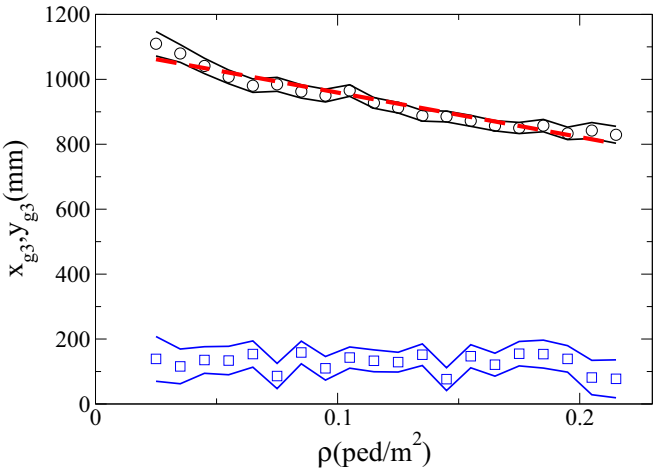

FIG. 8. (Color online) Black circles: ρ dependence of x_{g3} [Eq. (15)], compared to a linear fit of the data (dashed red). Blue squares: ρ dependence of y_{g3} [Eq. (16)]. Continuous lines provide standard error confidence intervals.

As shown in Fig. 7, the probability distribution for the extension of the group in the walking direction is centered around 0, i.e., the group walks in an abreast configuration,[13] while the spread of the distribution appears to grow slightly with increasing density.

C. Three-person groups

Figure 8 shows the density dependence of x_{g3} [Eq. (15)], compared to a linear fit of the average value data points,[14] and of y_{g3} [Eq. (16)]. The average abreast extension of the group is again decreasing with growing ρ and, while the effect seems to be weaker for higher density, the linear approximation is still a good one in the observed range. The probability distributions for x_{g3} are shown in Fig. 9, where we can see that with growing densities the bulk of the distribution is displaced toward lower x values; furthermore, for high ρ the probability distribution becomes narrower and more peaked.

From Fig. 8, showing that y_{g3} always assumes a positive average value, and from the y_{g3} probability distributions shown in Fig. 10, we may see that three-person groups have a strong tendency to walk in a V formation regardless of ρ. We may also observe that while at higher density the probability distribution maximum is found at a higher y, this effect is counterbalanced by a higher probability of finding the group in a Λ configuration, i.e., with negative y, and as a result

[13] We have nevertheless evidence of a very weak left-right asymmetry, as discussed in Sec. IV D.

[14] Given by $x_{g3} = \alpha + \beta\rho$, with $\alpha = 1.096$ m and $\beta = -1.370$ m^3/ped, and determination coefficient $R^2 = 0.939$.

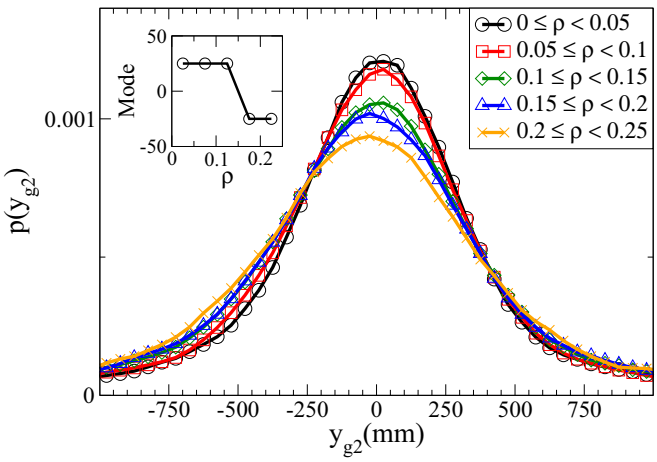

FIG. 7. (Color online) Probability distributions for y_{g2} [Eq. (14)] in different ρ ranges. The inset graph shows the position of the mode as a function of ρ. A one-way ANOVA analysis shows that the distributions in the figure are not different in a statistically significant way ($p \approx 0.35$).

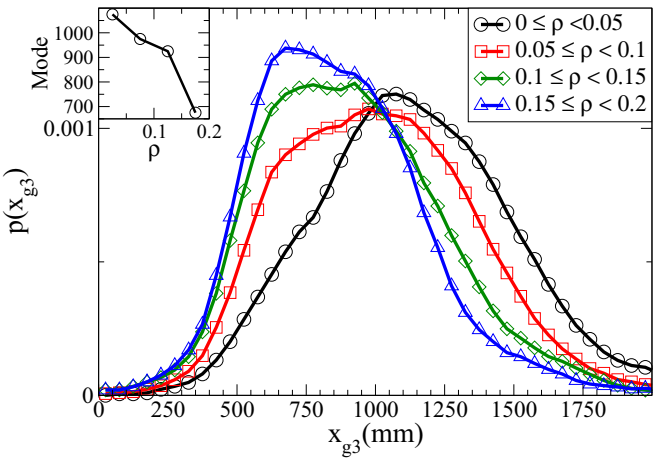

FIG. 9. (Color online) Probability distributions for x_{g3} [Eq. (15)] in different ρ ranges. The inset graph shows the position of the mode as a function of ρ. A one-way ANOVA analysis shows that the distributions in the figure are different in a statistically significant way ($p < 10^{-8}$).

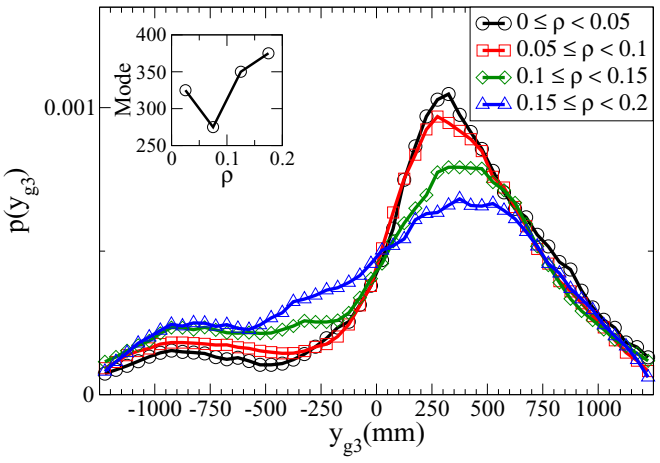

FIG. 10. (Color online) Probability distributions for y_{g3} [Eq. (16)] in different ρ ranges. The inset graph shows the position of the mode as a function of ρ. A one-way ANOVA analysis shows that the distributions in the figure are not different in a statistically significant way ($p \approx 0.87$). On the other hand, the overall empirical distribution in $\rho < 0.2$ ped/m^2 has an average value 140 ± 14 mm, with a $p < 10^{-8}$ value corresponding to the abreast configuration $y_{g3} = 0$.

the average value of the distribution is not affected in a significant way. The change in 2D structure of three-person groups under different density conditions is shown by the probability distributions of Fig. 11.

These results strongly suggest that also the V formation, described in [14] as characteristic of the $\rho \to 0$ group behavior, is very stable under changes in crowd density, with no significant variation with ρ in the average value of the distribution. This result is somehow different from the one described in [11], according to which three-person groups walk abreast at low density, and gradually "close" themselves in a more pronounced V formation at higher densities.

D. Left-right asymmetry

The probability distributions of Fig. 11, and in particular the high-density one, suggest a left-right asymmetry in three-person groups, possibly related to the tendency of Japanese pedestrians to walk on the left side of corridors, while

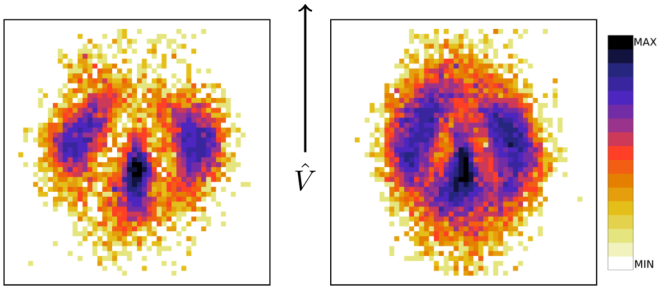

FIG. 11. (Color online) 2D probability distributions for the position in a three-person group in a 2.5-m-wide square centered on **X**. Left: $0 \leqslant \rho < 0.05$; right: $0.1 \leqslant \rho < 0.15$. The arrow shows the direction of motion of the group $\hat{\mathbf{V}}$.

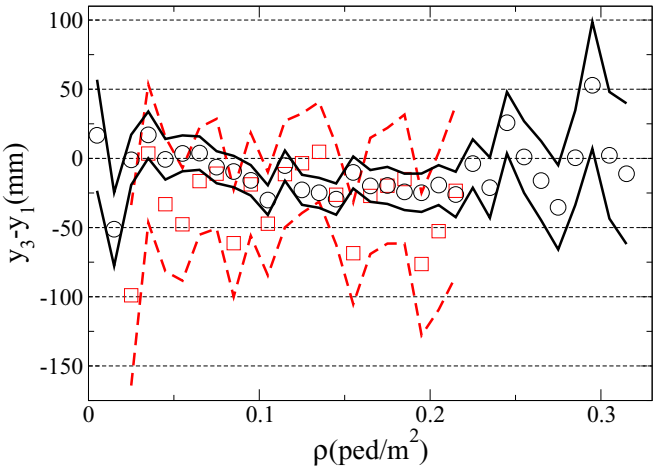

FIG. 12. (Color online) Black circles: ρ dependence of y_{g2} [Eq. (14)]. Continuous lines provide standard error confidence intervals. Red squares: ρ dependence of $y_3 - y_1$ for three-person groups. Dashed lines provide standard error confidence intervals.

overtaking on the right [28]. We may thus expect that three-person groups, by being slower than the rest of the crowd, find themselves close to the corridor's left limit. The pedestrian on the left is thus mainly interacting with the wall, while the one on the right interacts with the counterflow and with overtaking faster pedestrians. It is not surprising, then, that such an asymmetry arises. Figure 12 shows the ρ dependence of $y_3 - y_1$, which has indeed a tendency to assume a negative value, along with the ρ dependency of the extension in the direction of walking for two-person groups y_{g2} [Eq. (14)], which shows a similar tendency on an extended ρ range. While this effect is not particularly strong,[15] it could be due to the interaction of many features of pedestrian behavior (group behavior, avoidance and overtaking biases, interaction with walls), and thus it may be extremely useful in the calibration of the relative strengths of these components in a pedestrian model.

V. CONCLUSIONS AND FUTURE WORK

We observed that, keeping other conditions fixed, the abreast extension of two- and three-pedestrian walking social groups decreases with density, with a law that, in the investigated density range, may be considered in good approximation as linear. We have also verified that pedestrians walk in a V formation for all ρ values, and that the average distance between the front and back pedestrians does not depend on density. Furthermore, we have studied the ρ dependence of the individual and group velocities, and we verified that, regardless of density, groups are slower than individuals, and three-person groups are slower than two-person ones;

[15]For y_{g2}, the overall empirical distribution in $\rho < 0.3$ ped/m^2 has an average value -8.6 ± 4.5 mm, with a $p \approx 0.05$ value corresponding to the abreast configuration $y_{g2} = 0$, while for $y_3 - y_1$ the overall empirical distribution in $\rho < 0.2$ ped/m^2 has an average value -25 ± 16 mm, with a $p \approx 0.13$ value corresponding to the abreast configuration $y_3 = y_1$.

the difference between two- and three-person velocities is considerably smaller than that between individuals and two-person groups.

The main predictions of the model introduced in [14] for the behavior of groups in the low-density regime, namely the V formation structure of three-person groups and the decrease in group velocity with the increase in group size, are not disrupted by an increase in density. This result suggests that the effect of density, i.e., the reduction in the group spatial extension, could be modeled perturbing the potential of Eq. (1) by adding a simple, ρ-dependent, *effective potential*, following the approach sketched in [29].

A decrease in the spatial extension of groups is predicted also by the model introduced in [11]. Nevertheless, this model predicts that three-person groups walk in abreast configurations under low-density conditions, while at higher densities they assume a V formation, i.e., the extension of the groups in the walking direction should increase at higher density, a result that appears to be in contrast with that of Fig. 8. Although in Appendix E we perform a quantitative comparison between the empirical observations reported in this work and the prediction of the model presented in [14], at least for two-person groups and in the low-density range, a complete understanding of the relation between models [11,14] (and possibly other models of group behavior) and the empirical results introduced in this work would require a systematic simulation of the models under different density conditions, a task that we are planning to perform in the future.

We may nevertheless propose an interpretation of the empirical results based on the framework of our mathematical model [14]. According to it, both the V formation and the differences in velocity between groups of different size emerge due to the group internal dynamics, namely to the load of having to hold a conversation while walking toward a goal. As shown in Fig. 3, at high density the difference between the velocity of individuals, two-person, and three-person groups becomes smaller. This suggests that at high density groups are starting to "give up" their social interaction (since social interaction is directly connected to slowing down), for example in the case of three-person groups by assuming more often a Λ formation (see also Fig. 10), and in the case of two-person groups by walking more often in a line (see Fig. 6). This "switching" between a socially interacting mode and more collision avoidance oriented configurations could be modeled in a fashion similar to that proposed in [18].

It could be that at densities much higher than those examined in this work, groups do not present any preferred configuration, and pedestrians in groups limit themselves to stay spatially close to each other, as it is usually assumed in theoretical studies of the effect of groups on evacuation dynamics (see, for example, [30]). We may expect a crowd composed of groups that try to preserve a spatial configuration (i.e., actively interacting groups) to have a dynamics considerably different from a crowd with groups that just try to be spatially close. The transition between these two behaviors may thus be very relevant in the study of issues related to crowd security and event planning, and it deserves to be studied in greater detail.

We finally notice that the quantitative findings of this work related to the group spatial extension in the $\rho \to 0$ limit are different from those reported in [14], namely groups being smaller in abreast extension, as discussed in detail in Appendix E. This is probably due to the fact that the data used for the current paper were collected in a relatively narrow environment with an ongoing commercial activity, i.e., far from the almost ideal, *free walking* conditions of the environment in which the data used in [14] were collected (a wide, straight corridor without shops). We are now planning to collect new data to understand the effect of environmental features (and possibly also of group composition) on group dynamics.

Nevertheless, we believe that in this work we have shown clearly the effects of local density (while keeping all other variables fixed) on group behavior, and that our quantitative empirical findings may be of great help in the development of microscopic pedestrian models aimed to obtain reliable and realistic crowd simulations.

ACKNOWLEDGMENTS

We are grateful to Sayaka Taniguchi for the time- and energy-consuming labeling work, and to Zeynep Yücel for helping in the preparation of Figs. 2 and 11, reading the manuscript, and providing useful comments. We finally thank the anonymous reviewers, whose comments helped us to improve the quality of our work.

APPENDIX A: DEFINITION OF DENSITY

In thermodynamics or fluid dynamics, density is defined by averaging over volumes *small compared to the size of the system, but large compared to the size of the molecules*. This approach cannot be trivially extended to microscopic pedestrian studies, since using a volume (or better a surface) considerably larger than pedestrian size would mean losing most of the local information about how density influences individual behavior. Different solutions, such as Gaussian kernel methods [31] and Voronoi diagrams [32], have been proposed, but there is still no universal agreement in the field about how to define density.[16]

In this work, we have decided to use a very simple method. We divided space in square cells of fixed area $A = L^2$, and we counted all pedestrians that were tracked on each cell in a time interval T. Assuming T involved N observations, i.e., $T = N\Delta t$, and that n pedestrians were observed in the area during T, the density of the cell during the time interval T was defined as

$$\rho = \frac{n}{NA}. \tag{A1}$$

We assume the density felt by a pedestrian located in (continuous) position $\mathbf{x}$ and time t to be the density of the corresponding discrete cell of size L and time interval of length T. If at a given time pedestrians in the same group are located on different cells, the density perceived by the group is redefined as the average of the densities perceived by the group members.

[16]The reader may refer to [32] for a comparison of different methods in the measurement of straight corridor and T-junction fundamental diagram relations.

It is clear that it is impossible to obtain at the same time a high temporal and spatial resolution. If, for example, we use a value of L comparable to the pedestrian body size, and a value of T comparable to the observation time Δt, we have either one or zero pedestrians on the cell. In this work, we preferred to have a good spatial resolution, and we used $L = 0.5$ m, $T = 300$ s.[17] Furthermore, to compute density we used only data points in which the pedestrian velocity satisfied $v > 0.5$ m/s and from pedestrians that were tracked in a stable way, i.e., for at least 8 s and with an average vectorial velocity (total displacement over time) larger than 0.5 m/s. This choice, discussed in [24,27], was performed to avoid counting false pedestrian detections, due to the change of the structure of the environment, related to local commercial activity, with respect to the tracking system background,[18] and it is based on a comparison between the overall velocity and tracking time distributions in the tracking system output, and the distributions for explicitly coded pedestrians. Obviously, by using this filter, we remove also actual standing pedestrians. Nevertheless, we may expect standing pedestrians not to be located in the middle of the corridor, where most of the pedestrian flux happens, so that, since we limited ourselves to the study of moving groups and used cells with linear size small with respect to the size of the corridor, we may expect the removal of standing pedestrians not to affect our results. The validity of this assumption is tested by using a completely different density definition in Appendix D.

APPENDIX B: AVERAGES AND CONFIDENCE INTERVALS

Figures 3–5, 8, and 12 actually show the *average over group averages* values for the corresponding observables. They are computed in the following way. We define density slots of width $\Delta\rho$, i.e., with values ranging in

$$\rho_i - \Delta\rho/2 \leqslant \rho < \rho_i + \Delta\rho/2. \tag{B1}$$

Then for each group (or individual, in the case of Fig. 3) we average the value of the observable in each slot.[19] Finally, we average over all groups to obtain the data shown in the figures.[20] By considering different groups as statistically independent, we define standard errors as $\sigma_i/\sqrt{n_i}$, where σ_i is the variance (of the average over groups) of the observable in the slot i, and n_i is the number of groups observed in the slot. Only density slots that have data points from at least 100 groups were used to compute averages and confidence intervals. Linear fits are computed using just the data points shown in the graphs, i.e., using only the averages over averages. The corresponding determination coefficient values thus show how well a linear law describes average data points, without taking into consideration the deviations around the average in each density slot. The same approach, i.e., performing an average on data points from the same group in order to obtain statistically independent samples, is used also in the computation of p values in Figs. 6, 7, 9, 10, and Sec. IV D. In all the p value computations, including those in which the whole ρ average was compared to the abreast walking condition, group averages have been performed on $\Delta\rho = 0.05$ slots, and data from the same group in different slots were considered as independent.

It is useful to know how many groups were used to compute the data shown in the main text; this information is reported in Fig. 13.[21] Figure 14 shows the corresponding number of *overall data points* (i.e., counting possibly more than one observation for each group).

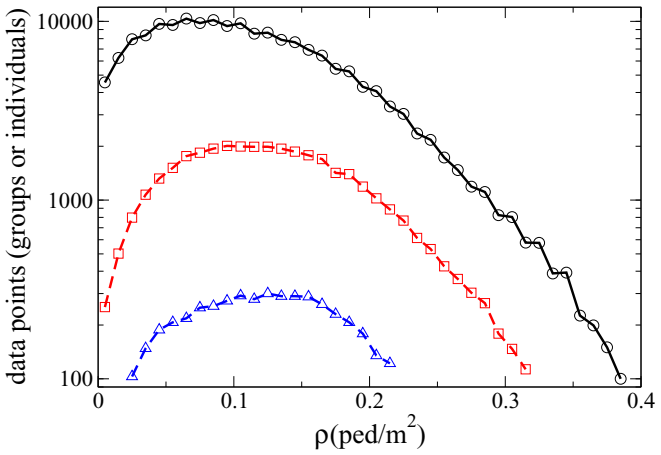

FIG. 13. (Color online) Data points used for Figs. 3–5, 8, and 12. Black circles: number of individual pedestrians (i.e., pedestrians not explicitly coded as part of groups) for each density slot. Red squares: number of two-person groups. Blue triangles: number of three-person groups.

APPENDIX C: PROBABILITY DISTRIBUTIONS

The probability distribution graphs of Figs. 6, 7, 9–11, 17, and 18 use larger density slots and are based on a computation, for each slot and observable, of the distribution histogram, which is then normalized in such a way to give an integral equal to 1. Finally, in the case of 1D graphs, continuous curves are obtained through a five-step, equal weight moving average. Data points are shown at the center of the original histogram slot. The number of data points used for each density slot may be found in Fig. 15.

[17] This choice gives us reasonable density values provided that the usage pattern of the environment does not change in a time scale short with respect to T.

[18] Our tracking system is provided with a semiautomatic background correction, and, at the time of each experiment, an operator was present to assess this problem. Nevertheless, considering also that the tracking experiment consisted of more than 800 h, a time lapse could pass between the background change and the operator action, causing such false detections. Refer to [23] for further details.

[19] The same group may contribute to multiple slots.

[20] Each data point is shown for $\rho = \rho_i$, i.e., at the center of the density slot.

[21] Very small differences are actually present between the number of data points used for Fig. 3 and those used for the other figures, since for the computation of velocities we used different filtering criteria to account for the need to remove false detections of individual pedestrians.

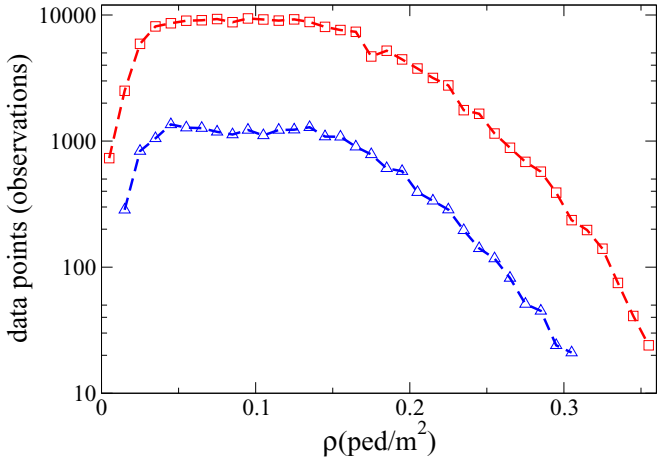

FIG. 14. (Color online) Red squares: number of two-person group data points (total number of observations) for each density slot. Blue triangles: number of three-person group data points (total number of observations) for each density slot.

APPENDIX D: A DIFFERENT DENSITY DEFINITION

The specific form of the law for the group abreast extension shrinking may depend on the definition of density. While for the main text we used a method with a good spatial resolution, here we may try to introduce a method with a high time resolution. To obtain Fig. 16, we defined density by counting all pedestrians present at a given time t in a rectangular area centered on the group center $\mathbf{X}$, with length 6 m in the direction of the group velocity $\mathbf{V}$, and width 4 m in the direction orthogonal to velocity, and then dividing by the area, without time average or velocity filters.[22] Figure 16 shows the comparison of the ρ dependence of x_{g2} using the two

[22]The averaging area may include walls and other places not accessible to pedestrians.

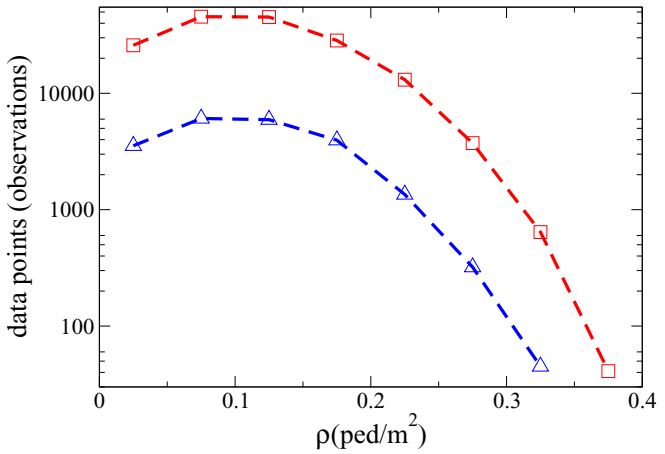

FIG. 15. (Color online) Data points used for Figs. 6, 7, and 9–11. Red squares: number of two-person group data points (number of observations) for density slot. Blue triangles: number of three-person group data points (number of observations) for density slot.

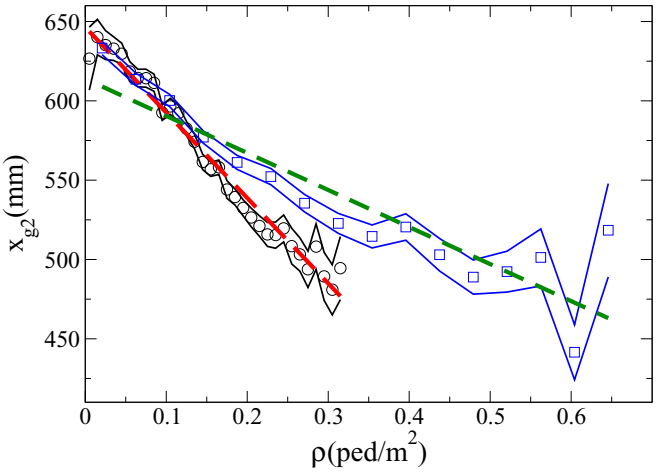

FIG. 16. (Color online) Dependence of x_{g2} on density. Black circles: ρ computed using cells with $A = 0.25$ m^2, $T = 300$ s, and data points with $v > 0.5$ m/s (linear fit in dashed red). Blue squares: ρ computed using cells with $A = 24$ m^2, $T = 0.5$ s, and all data points (linear fit in dashed green, with $\alpha = 0.614$ m, $\beta = -0.234$ m^3/ped, and $R^2 = 0.831$).

definitions (average over group averages and corresponding linear fits). We may notice the following:

(i) The high temporal resolution method, by not performing a time average and counting all pedestrians, smears density over a larger range.

(ii) Both methods show the group abreast extension as a decreasing function of density.

(iii) For the high temporal resolution method, the linear fit fails in describing the whole density range, since the convexity of the function manifests itself.

APPENDIX E: QUANTITATIVE COMPARISON TO EQ. (1)

We have seen that some of the features implied by the potential of Eq. (1) in the $\rho \to 0$ limit and for a large environment, namely Eqs. (3), (4), (5), and the V formation for three-person groups, hold qualitatively also at higher densities and for a relatively narrow corridor.

We may then wonder whether the potential of Eq. (1) correctly describes in a quantitative way the behavior of the pedestrians in the narrow corridor studied in this work, at least in the low-density regime. To verify if this is the case, we repeat the analysis performed in [14], which we recall briefly, inviting the interested reader to refer to the original work. By assuming that the effect of the environment on pedestrians in the group, including collision avoidance toward pedestrians outside the group, may be modeled as white noise,[23] we can derive for a pedestrian in a two-person group a Langevin equation in which the conservative deterministic force is given by the negative gradient of the potential of Eq. (1) with $\eta = 0$. As a result, we expect to have, for the probability distribution of the position relative to the group center $\mathbf{r}$ of a pedestrian in a two-person

[23]This is the essence of the low-density, large environment condition.

TABLE I. Model parameters obtained calibrating on all data in the $0 \leqslant \rho < 0.05$ ped/m^2 range by using Eq. (E3) for the ATC and [14] data sets. r_0 in m, T in m^2/s^2.

	$\tilde{\varepsilon}$	r_0	C_r/C_θ	T
ATC	0.49	0.67	7.5	0.13
[14]	0.38	0.75	9.0	0.057

group,

$$p_T(\mathbf{r}) \propto \exp[-U^0(2\mathbf{r})/T], \tag{E1}$$

where the "temperature" T is determined by the intensity of the stochastic term in the Langevin equation. By comparing p_T with the empirically observed probability distribution p_E, or better by minimizing the relative error weighted by the number of observations per cell on the discrete grid on which p_E is defined as

$$\varepsilon \equiv \sum_{i,j\in\text{cells}} \frac{[p_T(x_i,y_j) - p_E(x_i,y_j)]^2}{p_E(x_i,y_j)}, \tag{E2}$$

we may find the parameters r_0 and C_r/C_θ in Eq. (1) and the temperature T that better describe the data.

A straightforward application of this approach does not allow us to take into account the influence of the environment. To do that, we may nevertheless follow the method used by [8], and calibrate on

$$\tilde{\varepsilon} \equiv \sum_{i,j\in\text{cells}} \frac{[p_T(x_i,y_j) - \tilde{p}_E(x_i,y_j)]^2}{\tilde{p}_E(x_i,y_j)}, \tag{E3}$$

where

$$\tilde{p}_E(\mathbf{r}) \equiv p_E(\mathbf{r})/p_{\text{NI}}(\mathbf{r}), \tag{E4}$$

and $p_{\text{NI}}(\mathbf{r})$ is the distribution of distances between noninteracting pedestrians (i.e., outside groups) walking in the same direction,[24] which we may calculate from the probability distribution of pedestrian positions in the environment.[25]

Since $p_T(\mathbf{r})$ is calibrated on $\tilde{p}_E(\mathbf{r})$, we cannot compare it directly to the empirical distribution $p_E(\mathbf{r})$, and thus we may define a *calibrated distribution* $p_C(\mathbf{r})$ for which such a comparison is possible, i.e.,

$$p_C(\mathbf{r}) \equiv p_T(\mathbf{r})\, p_{\text{NI}}(\mathbf{r}). \tag{E5}$$

By using data points in the $0 \leqslant \rho < 0.05$ ped/m^2 range, we obtain, for the ATC and [14] data sets, the parameter values shown in Table I. The increased value of the temperature is easily explained by the fact that the ATC environment is less regular (not straight, presence of shops) and thus more "noisy,"

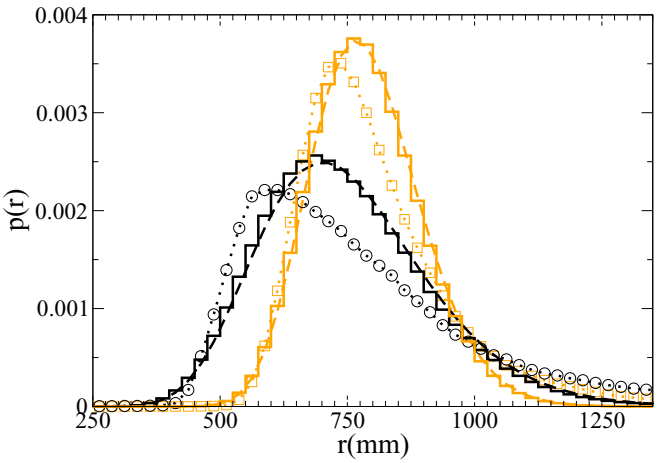

FIG. 17. (Color online) Comparison between the empirical $p_E(r)$, theoretical $p_T(r)$, and calibrated $p_C(r)$ distributions in both data sets. For the ATC set, the black dotted line and circles represent $p_E(r)$, the black dashed line represents $p_T(r)$, and the black histogram represents $p_C(r)$. For the [14] set, the orange (gray) dotted line and squares represent $p_E(r)$, the orange dashed line represents $p_T(r)$, and the orange histogram represents $p_C(r)$. All data refer to densities in the $0 \leqslant \rho < 0.05$ ped/m^2 range.

in the sense of the Langevin equation introduced in [14]. We notice nevertheless that, despite our redefinition of the probability distribution in Eq. (E4), the values of the other parameters are similar but different, and in particular pedestrians walk closer in the narrow corridor. While $p_{\text{NI}}(\mathbf{r})$ accounts for a reduced probability of noninteracting pedestrians to have a large "abreast distance," this effect is too weak to account for the closer distance at which pedestrians in two-person groups walk. This could be due to the fact that the effect of the environment on groups is qualitatively different from the effect on individuals, due to the peculiar spatial structure and velocity of the former. This point should be investigated numerically,[26] a task that we leave for a future work.

The value of $\tilde{\varepsilon}$ [Eq. (E3)] was roughly 30% higher for the ATC data set compared to the data set of [14], implying a reduced capability of the model to describe the data.

Figure 17 shows a comparison, in both environments, between $p_E(r)$, $p_T(r)$, and $p_C(r)$, where $p_E(r)$ is the empirical probability distribution for the distance between pedestrians in a two-person group, $p_T(r)$ is the theoretical distribution derived by the distribution $p_T(\mathbf{r})$ [i.e., the one calibrated with Eq. (E3)] and satisfies [using Eqs. (1) and (E1)]

$$\begin{aligned} p_T(r) &\propto r \exp[-R(r)/T] \int d\theta \exp[-\Theta^0(\theta)/T] \\ &\propto r \exp[-R(r)/T], \end{aligned} \tag{E6}$$

while $p_C(r)$ is computed by numerically integrating over $p_C(\mathbf{r})$ in Eq. (E5).

[24] Since in a corridor the pedestrian spatial distributions depend on the walking direction [28].

[25] In detail, we divide pedestrians out of groups according to their walking direction in the corridor, and for each direction we compute, on a sufficiently refined grid, the probability of finding a pedestrian and the average velocity vector. We may use the velocity vector to define a local frame, and compute $p_{\text{NI}}(\mathbf{r})$ by integrating on the whole corridor distances between points randomly selected using the spatial probability distribution.

[26] By running a microscopic simulation of a corridor with individuals and groups, with realistic collision avoidance between pedestrians and with walls.

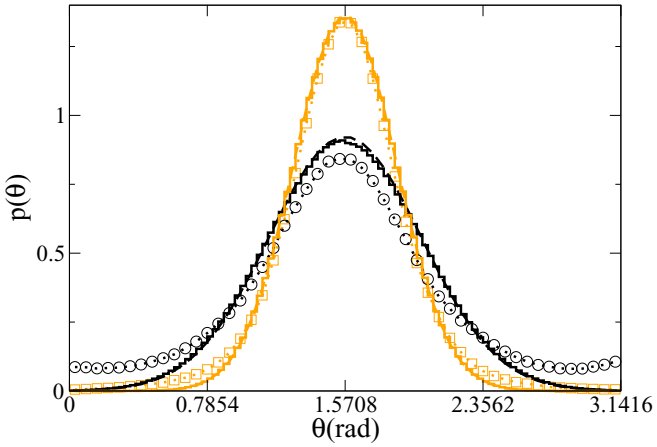

FIG. 18. (Color online) Comparison between the empirical $p_E(\theta)$, theoretical $p_T(\theta)$, and calibrated $p_C(\theta)$ distributions in both data sets. For the ATC set, the black dotted line and circles represent $p_E(\theta)$, the black dashed line represents $p_T(\theta)$, and the black histogram represents $p_C(\theta)$. For the [14] set, the orange (gray) dotted line and squares represent $p_E(\theta)$, the orange dashed line represents $p_T(\theta)$, and the orange histogram represents $p_C(\theta)$. All data refer to densities in the $0 \leqslant \rho < 0.05$ ped/m^2 range, and they are limited to $0 \leqslant \theta < \pi$.

Figure 18 performs the same comparison between the θ distributions, where

$$p_T(\theta) \propto \exp[-\Theta^0(\theta)/T]. \tag{E7}$$

The averages, standard deviations, and modes for the empirical p_E and calibrated p_C distributions are shown in Table II.

We may notice that the p_T and p_C distributions are hardly distinguishable, showing that the variation in $p_{\rm NI}$ is too slow with respect to the variation in p_T to have a significant effect. We also notice that the proposed potential still describes qualitatively well the position and shape of the main bulk of the r and θ distributions, although the position and shape of the r peak are clearly identified less well for the ATC data set.[27] Regarding the tail of the r distribution, the model underestimates the probability of finding pedestrians at a distance considerably larger than r_0, but its performance is not very different between the two data sets. On the other hand, the model fails in describing the relatively high probability of having pedestrians walking in a line ($\theta \approx 0,\pi$) in the ATC data set, and thus the description of the θ distribution is not as good as for the data set of [14].

TABLE II. Average value r and θ (with standard deviations) and modes $\overline{r}$, $\overline{\theta}$ for the two-person empirical distributions $p_E(r)$ and $p_E(\theta)$, and for the calibrated distributions $p_C(r)$ and $p_C(\theta)$ shown in Figs. 17 and 18. r variables in m, θ in radians. The statistics for θ is limited to $0 \leqslant \theta < \pi$.

	ATC p_E	ATC p_C	[14] p_E	[14] p_C
r	0.82 ± 0.32	0.74 ± 0.16	0.82 ± 0.19	0.79 ± 0.11
$\overline{r}$	≈ 0.60	≈ 0.67	≈ 0.73	≈ 0.76
θ	1.56 ± 0.57	1.57 ± 0.44	1.57 ± 0.34	1.57 ± 0.29
$\overline{\theta}$	$\approx \pi/2$	$\approx \pi/2$	$\approx \pi/2$	$\approx \pi/2$

As discussed in detail in [14], the proposed model, which is a model for *socially interacting pedestrians*, assigns always a very low probability to have pedestrians not moving in an abreast configuration.[28] In an environment with reduced space, in order to perform collision avoidance, the pedestrians may need to suspend their social interaction and switch to a following behavior (walking in a line). The results of Fig. 18 strongly suggest that this cannot be obtained simply by summing the dynamics of Eq. (1) with a collision avoidance force, and an explicit coding of the "walking in a line" behavior is necessary.[29] A similar approach has been described in [18].

[27] This is probably due to the inability of Eq. (E4) to fully include the effect of the environment.

[28] Unless different values of η in Eq. (1) are assigned to each pedestrian. In particular, if one pedestrian has an $\eta > 0$ and the other one $\eta < 0$, the latter will follow the former.

[29] For example, by changing the η parameters, as discussed in the previous footnote.

[1] L. Henderson, Nature (London) **229**, 381 (1971).
[2] P. P. Kachroo, S. J. Al-Nasur, and S. A. Wadoo, *Pedestrian Dynamics: Feedback Control of Crowd Evacuation* (Springer, Berlin, 2008).
[3] M. Muramatsu and T. Nagatani, Physica A **286**, 377 (2000).
[4] C. Burstedde, K. Klauck, A. Schadschneider, and J. Zittartz, Physica A **295**, 507 (2001).
[5] D. Helbing and P. Molnar, Phys. Rev. E **51**, 4282 (1995).
[6] S. Hoogendoorn and W. Daamen, Traffic Granular Flow **03**, 373 (2005).
[7] T. Kretz, A. Grünebohm, M. Kaufman, F. Mazur, and M. Schreckenberg, J. Stat. Mech.: Theor. Exp. (2006) P10001.
[8] I. Karamouzas, B. Skinner, and S. J. Guy, Phys. Rev. Lett. **113**, 238701 (2014).
[9] D. Helbing and A. Johansson, Encycl. Complex. Syst. Sci. **16**, 6476 (2009).
[10] M. Schultz, L. Rößger, H. Fricke, and B. Schlag, in *Pedestrian and Evacuation Dynamics 2012* (Springer, Berlin, 2014), pp. 1097–1111.
[11] M. Moussaïd, N. Perozo, S. Garnier, D. Helbing, and G. Theraulaz, PLoS One **5**, e10047 (2010).
[12] M. Costa, J. Nonverbal Behav. **34**, 15 (2010).
[13] F. Zanlungo and T. Kanda, in *COGSCI13* (Cognitive Science Society, Austin, TX, 2013).
[14] F. Zanlungo, T. Ikeda, and T. Kanda, Phys. Rev. E **89**, 012811 (2014).
[15] H. Klüpfel, in *Pedestrian and Evacuation Dynamics 2005* (Springer, Berlin, 2007), pp. 285–296.

[16] M. Schultz, C. Schulz, and H. Fricke, in *Pedestrian and Evacuation Dynamics 2008* (Springer, Berlin, 2010), pp. 381–396.
[17] G. Köster, M. Seitz, F. Treml, D. Hartmann, and W. Klein, Contemp. Soc. Sci. **6**, 397 (2011).
[18] I. Karamouzas and M. Overmars, in *Proceedings of the 17th ACM Symposium, VRST* (ACM, New York, 2010), pp. 183–190.
[19] Y. Zhang, J. Pettré, X. Qin, S. Donikian, and Q. Peng, in *CAD/Graphics 2011* (IEEE, Piscataway, NJ, 2011), pp. 275–281.
[20] L. Cheng, R. Yarlagadda, C. Fookes, and P. K. Yarlagadda, World **1**, 002 (2014).
[21] G. Turchetti, F. Zanlungo, and B. Giorgini, Europhys. Lett. **78**, 58003 (2007).
[22] J.-a. Xi, X.-l. Zou, Z. Chen, and J.-j. Huang, Transport. Res. Proc. **2**, 60 (2014).
[23] D. Brščić, T. Kanda, T. Ikeda, and T. Miyashita, IEEE Trans. Human-Machine Syst. **43**, 522 (2013).
[24] D. Brščić, F. Zanlungo, and T. Kanda, Transport. Res. Proc. **2**, 77 (2014).
[25] M. L. Knapp, *Nonverbal Communication in Human Interaction* (Cengage Learning, Stamford, CT, 2012).
[26] C. L. Kleinke, Psych. Bull. **100**, 78 (1986).
[27] F. Zanlungo, Y. Chigodo, T. Ikeda, and T. Kanda, in *Pedestrian and Evacuation Dynamics 2012* (Springer, Berlin, 2014), pp. 289–304.
[28] F. Zanlungo, T. Ikeda, and T. Kanda, PloS One **7**, e50720 (2012).
[29] F. Zanlungo, D. Brščić, and T. Kanda, Transport. Res. Proc. **2**, 149 (2014).
[30] F. Müller, O. Wohak, and A. Schadschneider, Transport. Res. Proc. **2**, 168 (2014).
[31] D. Helbing, A. Johansson, and H. Z. Al-Abideen, Phys. Rev. E **75**, 046109 (2007).
[32] J. Zhang, W. Klingsch, A. Schadschneider, and A. Seyfried, J. Stat. Mech.: Theor. Exp. (2011) P06004.